


Stochastic dynamics of a nonlinear thermal circuit with bistability

Qinli Ruan (阮琴丽) and Lei Wang (王雷)^{*}

Department of Physics and Beijing Key Laboratory of Opto-electronic Functional Materials and Micro-Nano Devices, Renmin University of China, Beijing 100872, People's Republic of China

 (Received 30 January 2023; accepted 2 April 2023; published 24 April 2023)

Stochastic dynamics of a nonlinear thermal circuit is studied. Due to the existence of negative differential thermal resistance, there exist two stable steady states that satisfy both the continuity and stability conditions. The dynamics of such a system is governed by a stochastic equation which describes originally an overdamped Brownian particle that undergoes a double-well potential. Correspondingly, the finite time temperature distribution takes a double-peak profile and each peak is approximately Gaussian. Owing to the thermal fluctuation, the system is able to jump occasionally from one stable steady state to the other. The probability density distribution of the lifetime τ for each stable steady state follows a power-law decay $\tau^{-3/2}$ in the short- τ regime and an exponential decay $e^{-\tau/\tau_0}$ in the long- τ regime. All these observations can be well explained analytically.

DOI: [10.1103/PhysRevE.107.044120](https://doi.org/10.1103/PhysRevE.107.044120)

I. INTRODUCTION

Due to the fundamental importance in statistical physics, studies on heat conduction in low-dimensional systems have led to impressive theoretical and experimental developments in recent years [1]. In particular, the field of phononics, which aims to control the directional flow of heat current by manipulating phonons, has attracted rapidly increasing interest [2] for its apparent value in practice. The model of a thermal diode [3], which rectifies heat current, presents the first step toward controlling the direction of heat flow. A model of a thermal transistor with efficient control of heat flows by means of temperature was then successfully designed [4]. It can be viewed as the “nerve cell” of the thermal circuit because it allows us to switch and modulate heat current, just like what we have been able to do for electric current. On this basis, thermal analogs of many other electronic devices, such as thermal logic gates [5] and thermal memory [6], were then worked out. The underlying mechanism of these models is match or mismatch of the phonon power spectra, which greatly controls the heat current that flows through an interface. This mechanism attracted extensive studies [7] and other mechanisms that realize the functions of thermal diode [8], thermal transistor [9], and thermal memory [10] were also proposed shortly. Recently some of them have already been experimentally implemented [11]. The idea of phononics, i.e., to control heat by heat, has also been extended to control sound by sound [12].

In all these devices, a nonlinear component must be necessary. It is well known that in a simple electric resistance circuit in which all the resistances are linear, i.e., the electric current flowing through is proportional to the voltage drop applied, i.e., $U = RI$, then the steady state satisfying all the Kirchhoff laws must be unique and this state must be stable. Whereas, if nonlinear resistance exists, there may exist

multiple steady states, some of which are stable. The system finally falls into which one of the stable steady states depends on the initial conditions [13]. Those facts are also true for a thermal circuit, i.e., in a linear thermal circuit in which each component satisfies $J = \Delta T/R$, where J denotes the heat current and ΔT denotes the temperature drop, the steady state of the circuit is also unique and stable. However, in contrast with the electric cases, for a nonlinear thermal circuit with multiple stable steady states, due to the thermal fluctuation, the system might jump randomly from one stable steady state to another. Such jumps present much richer physical pictures and thus give the system more practical significance, although they are detrimental for a thermal memory [6].

The existing studies on the thermal circuits basically focused on the statistical properties of those stable steady states themselves, but the crucial role of thermal fluctuation was commonly overlooked. In this paper, we go one step further and concentrate on the stochastic dynamics that induces the above-mentioned random jumps between the stable steady states. We present a one-dimensional (1D) Langevin equation that can describe the dynamics quite well.

The rest of this paper is arranged as follows: Section II is devoted to the introduction of the model of negative differential thermal resistance. In Sec. III we present our numerical findings, including the multiple steady states, probability distributions of the finite time temperature T_O , and the lifetime of stable steady states, as well as the autocorrelation of T_O . In Sec. IV, theoretical analyses are presented. All the findings can be well explained by the aforementioned Langevin equation. Discussion and conclusions are presented in Sec. V.

II. MODEL OF NONLINEAR THERMAL CIRCUIT

The key factor of a thermal transistor that can realize the functions of a thermal switch and a thermal modulator [4] is the so-called negative differential thermal resistance (NDTR), i.e., the lower the temperature drop, the higher the induced heat current. Compared with many later proposed models [14]

^{*}phywanglei@ruc.edu.cn

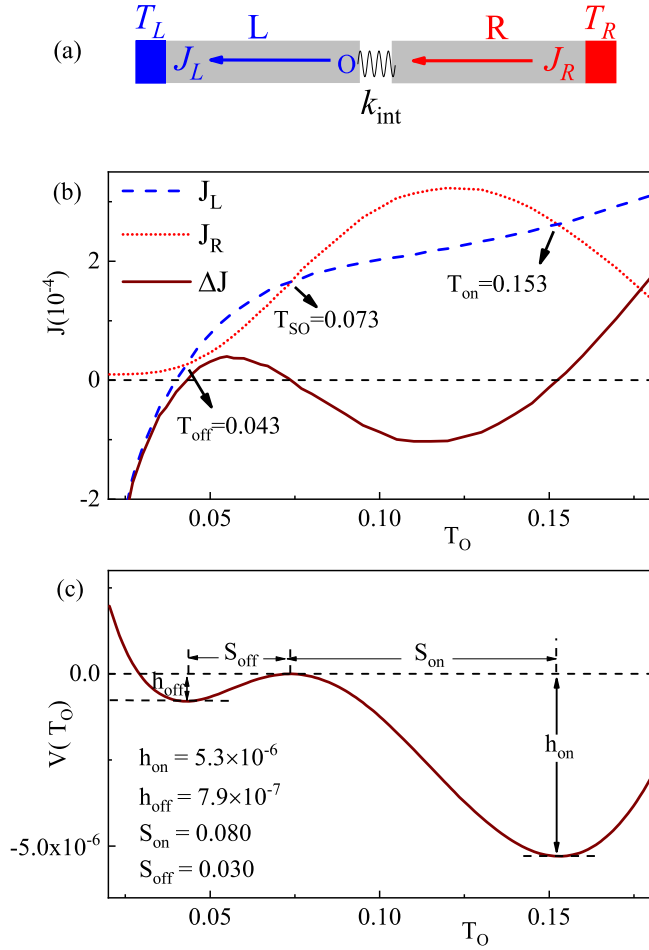


FIG. 1. (a) The setup of the model with NDTR. The positive directions of the heat currents J_L and J_R are illustrated. (b) Fundamental diagram of the system, i.e., the heat currents J_L , J_R , and the net heat current $\Delta J \equiv J_L - J_R$ versus temperature T_O . At three points $T_O = T_{\text{off}}$, T_{SO} , and T_{on} , $J_L = J_R$ thus $\Delta J(T_O) = 0$. (c) The corresponding potential $V(T_O)$ which satisfies $dV(T_O)/dT_O = \Delta J(T_O)$.

that realize NDTR, the original one which consists of two weakly coupled 1D Frenkel-Kontorova (FK) [15] segments is still one of the most effective. In this paper, a similar setup is still applied, see Fig. 1(a). The two FK segments, left and right, are with particle numbers N_L and N_R , respectively. Each segment is subjected to a periodic onsite potential with height V_L and V_R , respectively, and particles in each segment are coupled to their nearest neighbors by a linear spring with strength k_L and k_R , respectively. The two segments are coupled with a weak linear spring with strength k_{int} . The whole system can be described by the following Hamiltonian:

$$\begin{aligned}
 H &= H_L + H_R + H_{\text{int}} \\
 &= \sum_{i=1}^{N_L} \frac{1}{2} \dot{x}_{L,i}^2 + \frac{1}{2} k_L (x_{L,i} - x_{L,i-1})^2 - \frac{V_L}{(2\pi)^2} \cos 2\pi x_{L,i} \\
 &\quad + \sum_{i=1}^{N_R} \frac{1}{2} \dot{x}_{R,i}^2 + \frac{1}{2} k_R (x_{R,i} - x_{R,i-1})^2 - \frac{V_R}{(2\pi)^2} \cos 2\pi x_{R,i} \\
 &\quad + \frac{1}{2} k_{\text{int}} (x_{L,N_L} - x_{R,N_R})^2,
 \end{aligned} \tag{1}$$

where $x_{L,i}$ and $x_{R,i}$ indicate the particles' displacements relative to their equilibrium positions in the segments L and R , respectively. Fixed boundary conditions are applied, i.e., $x_{L,0} = x_{R,0} = 0$. The following parameters are applied: $N_L = N_R = 200$, $k_L = 0.83$, $k_R = 0.1$, $k_{\text{int}} = 0.038$, $V_L = 5.0$, $V_R = 0$. They are different from those we applied in all our previous studies [4,6,16]. Such choices clearly display the physical phenomena of interest, however, they do not affect the generality of the results. Two Langevin-type heat baths with temperatures $T_L = 0.04$ and $T_R = 0.2$ are always coupled to the ends of the two segments.

III. NUMERICAL RESULTS

In this section, various numerical simulations will be presented and all of the results are explained in the next section.

A. Fundamental diagram and macroscopic dynamics of the system

For the given fixed values of T_L and T_R , the stationary-state heat currents J_L and J_R illustrated in Fig. 1(a) are determined by the temperature T_O . We call such a dependence the fundamental diagram of the system [16]. It is the key feature of this device. To observe it, a third heat bath is attached to the particle O (particle N_L of the left segment) so as to fix its temperature to a desired value T_O , and the so-induced stationary-state heat currents J_L and J_R are measured. To do so, all the particles are initially set to their equilibrium positions and their velocities are set to random values which correspond to a temperature uniformly distributed within $[T_L, T_R]$. Each average is then taken over typically 5×10^7 time units, after a transient of 3×10^7 time units. The observed fundamental diagram is plotted in Fig. 1(b). In a wide regime of T_O , the heat current J_R can increase with T_O , which indicates NDTR, i.e., the lower the temperature drop $T_R - T_O$ the higher the induced heat current J_R . It is possible because the power spectrum of particle O depends sensitively on T_O . When T_O increases, it shifts leftwards and its match with that of the particle at the other side of the interface is largely enhanced [4], the heat current J_R is therefore enhanced, too, in despite of the decreasing temperature drop $T_R - T_O$. Due to the NDTR, the curves for J_L and J_R cross at three different points, which have been previously named the ‘‘on,’’ ‘‘semi-on’’ (SO), and ‘‘off’’ states [4]. $T_{\text{on}} = 0.153$, $T_{\text{off}} = 0.043$, and $T_{\text{SO}} = 0.073$. In these three states, $J_L = J_R$, so the third heat bath does not need to provide or absorb any heat current.

When the heat bath attached to the particle O is absent, the dynamics of the temperature T_O follows

$$C_O \frac{dT_O}{dt} = -J_l(T_O) + J_r(T_O) = -\Delta J(T_O) \equiv -\frac{dV(T_O)}{dT_O}, \tag{2}$$

where C_O denotes the heat capacity of particle O . Note that J_l and J_r , i.e., those with lowercase subscripts, denote the instantaneous heat currents. From the macroscopic point of view, in which thermal fluctuations are not considered, J_l and J_r should depend on the instantaneous temperature T_O only (for the given fixed T_L and T_R), i.e., they do not explicitly depend on time t . We suppose that this dependence still follows the fundamental diagram, which describes the dependence of J_L and J_R on the time-independent temperature T_O . Such a dynamics is equivalent to that of an overdamped particle

undergoing a potential $V(T_O)$, which has been illustrated in Fig. 1(c). According to the fundamental diagram shown in Fig. 1(b), $V(T_O)$ takes a double-well form, with two wells located at T_{on} and T_{off} . Any asymptotic solution of Eq. (2) must be a steady state that satisfies both the continuity condition

$$\Delta J(T_O) = 0, \quad (3)$$

and the stable condition

$$\Delta J'(T_O) \equiv \frac{\partial \Delta J(T_O)}{\partial T_O} > 0. \quad (4)$$

The continuity condition is satisfied in all the three key states: on, off, and semi-on. One can easily confirm that $\Delta J'(T_{\text{on}})$ and $\Delta J'(T_{\text{off}})$ are both positive, so these two states are stable steady states (SSSs). The system falls into one of them and stays there forever. In contrast, $\Delta J'(T_{\text{SO}})$ is negative, so the semi-on state is a unstable steady state (USS). The system will not stay there and will tend to one of the SSSs.

B. Microscopic dynamics and finite-time temperature

In the microscopic point of view, thermal fluctuations must be considered. Therefore, J_l and J_r do not simply equal $J_L(T_O)$ and $J_R(T_O)$ any longer. Noise terms should be added, i.e., $J_l(T_O, t) = J_L(T_O) + \xi_L(t)$ and $J_r(T_O, t) = J_R(T_O) + \xi_R(t)$. Consequently,

$$C_O \frac{dT_O}{dt} = -\frac{dV(T_O)}{dT_O} + \xi_L(t) + \xi_R(t). \quad (5)$$

Due to these noise terms, the system can possibly be kicked out of one SSS and then jumps to the other.

To observe such a process, a time-dependent temperature should be defined. It is well known that a global kinetic temperature can be defined as $T \equiv \langle \xi \partial_{\xi} H \rangle$ in an equilibrium state of a Hamiltonian system provided that ergodicity is satisfied, where ξ is any canonical coordinate of the system (p_i or q_i). The bracket denotes the long-time average. The simple choice of $\xi = p_i$ yields a definition of local kinetic temperature, i.e., $T_i \equiv \langle p_i \partial H / \partial p_i \rangle = \frac{1}{m_i} \langle p_i^2 \rangle$, provided that the local equilibrium is satisfied [17,18]. By removing the bracket, we may naturally define an instantaneous local temperature. However, since the dynamics of the system is governed by the Hamiltonian (1), each particle is basically vibrating around its equilibrium position, the so defined instantaneous temperature must be largely oscillating, so little useful information can be obtained. To solve this problem, we defined a finite-time temperature (of particle O), i.e., the average kinetic temperature in a finite time window δt [6,16],

$$T_O(t) \equiv \frac{1}{\delta t} \int_{t-\frac{\delta t}{2}}^{t+\frac{\delta t}{2}} v_O^2(t') dt'. \quad (6)$$

The same as applied in our previous studies [6,16], δt is fixed to 10^4 time units throughout this paper, which covers about 2000 oscillations of this particle.

In Fig. 2(a), a typical evolution of the finite-time temperature $T_O(t)$ is plotted. As expected, the system commonly stays around one SSS for quite a long period of time and then jumps to the other. The picture described by Eq. (5) is clearly confirmed.

To further understand the dynamics of $T_O(t)$ quantitatively, the probability density function (PDF) [6,16] of the finite-time

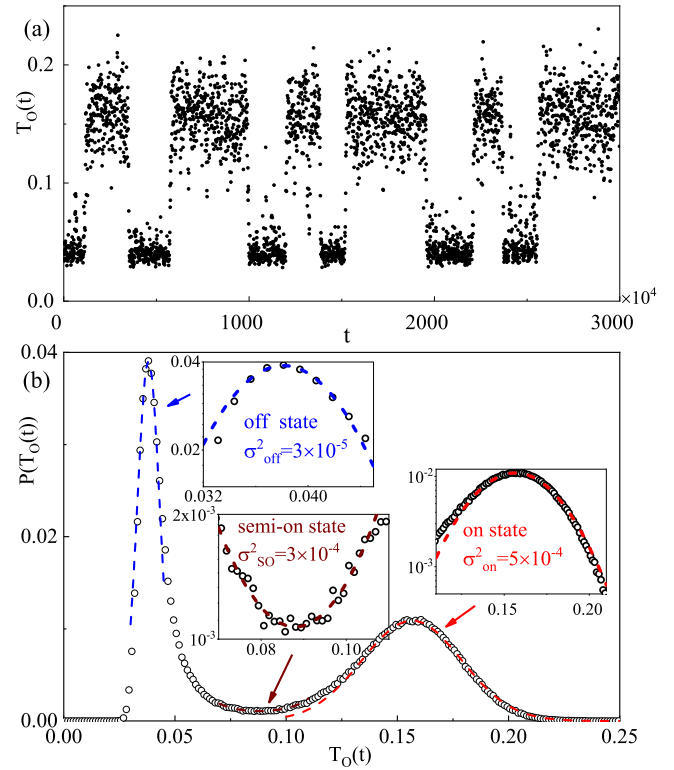


FIG. 2. (a) A typical evolution of the finite-time temperature $T_O(t)$. The long time stays around each SSS and also the random jumps between the two SSSs can be observed directly. (b) PDF of the finite-time temperature $T_O(t)$. Insets show blowups of the PDF around the three steady states in a single logarithmic plot. The symbols show the numerical data and curves show the local Gaussian fits described by the Eqs. (7)–(9). Those around the two SSSs take a Gaussian form, while the one around the USS takes an inverted Gaussian form.

temperature $T_O(t)$ is calculated, see Fig. 2(b). Since we study only the PDF of the finite-time temperature of this particle, the term “PDF” always refers to $P(T_O(t))$ hereafter. Not surprisingly, two peaks locate at T_{off} and T_{on} and a well located in between are clearly observed. Such an observation agrees well with the picture that the system stays around one SSS and then jumps occasionally to the other SSS. It is worth mentioning that, although it is expected that the local minimum of the PDF [in Fig. 2(b)] should locate at T_{SO} [in Fig. 1(b)], this is not exactly the case. The reason is that the simulations in the two figures are for different conditions, one with the third heat bath but the other without. However, such a slight difference does not affect the understanding of the physical picture, so we ignore it hereafter.

More exactly, we see that, around the three key points, T_{on} , T_{off} , and T_{SO} , the PDF satisfies the following fits quite well:

$$P(T_O) = P(T_{\text{on}}) e^{-\frac{(T_O - T_{\text{on}})^2}{2\sigma_{\text{on}}^2}}, \quad T_O \approx T_{\text{on}}, \quad (7)$$

$$P(T_O) = P(T_{\text{off}}) e^{-\frac{(T_O - T_{\text{off}})^2}{2\sigma_{\text{off}}^2}}, \quad T_O \approx T_{\text{off}}, \quad (8)$$

$$P(T_O) = P(T_{\text{SO}}) e^{-\frac{(T_O - T_{\text{SO}})^2}{2\sigma_{\text{SO}}^2}}, \quad T_O \approx T_{\text{SO}}, \quad (9)$$

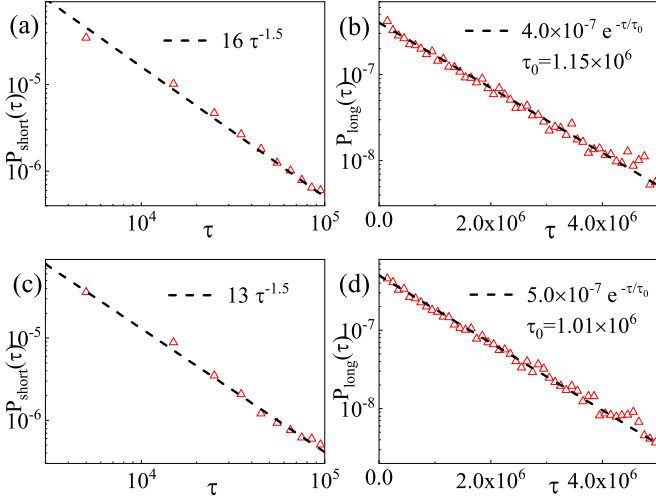


FIG. 3. The lifetime distribution $P(\tau)$ for on (upper row) and off (lower row) states. (a), (c) In the short- τ regime, the decay follows a power law with the power exponents both very close to -1.5 . (b), (d) In the long- τ regime, the decay changes to exponential.

where the variances $\sigma_{\text{on}}^2 = 5 \times 10^{-4}$, $\sigma_{\text{off}}^2 = 3 \times 10^{-5}$, and $\sigma_{\text{SO}}^2 = 3 \times 10^{-4}$ are positive constants. Namely, in a single logarithmic plot there are two Gaussian distributions and one inverted Gaussian distribution, see the insets of Fig. 2(b). All these observations are explained in Sec. IV.

C. Lifetime and its distribution of the stable steady states

Besides the PDF that presents the probability density of $T_O(t)$ that visits a temperature regime, we are also interested in how often the jumps happen, which measures quantitatively the stability of the SSS. It is crucial in making a thermal memory [6]. To study it, we define that the system is in the on (off) state if the finite-time temperature $T_O(t)$ is higher (lower) than a critical temperature $T_c = 0.085$. The duration time (lifetime) τ of each stay in a SSS, the probability density distribution of the lifetime $P(\tau)$, and the mean lifetime τ_{MEAN} can be then defined accordingly. The value of T_c is chosen so as to maximize the mean lifetime of the SSS. It is also the value where the PDF gets its local minimum. As mentioned above, T_c is close to but not exactly equal to T_{SO} .

In Fig. 3, $P(\tau)$ for the two SSSs is plotted. It behaves quite differently in the short- and long- τ regimes. In the short- τ regime, the decay of $P(\tau)$ satisfies a power law, and the power exponents are both very close to -1.5 , i.e.,

$$P_{\text{short}}(\tau) = 16 \tau^{-1.5}, \quad \text{for the on state,} \quad (10)$$

$$P_{\text{short}}(\tau) = 13 \tau^{-1.5}, \quad \text{for the off state,} \quad (11)$$

see Figs. 3(a) and 3(c), respectively. Whereas, in the long- τ regime, $P(\tau)$ decays exponentially, i.e.,

$$P_{\text{long}}(\tau) = 4.0 \times 10^{-7} e^{-\tau/\tau_0}, \quad \text{for the on state,} \quad (12)$$

$$P_{\text{long}}(\tau) = 5.0 \times 10^{-7} e^{-\tau/\tau_0}, \quad \text{for the off state,} \quad (13)$$

with $\tau_0 = 1.15 \times 10^6$ and 1.01×10^6 for the on and off states, respectively, see Figs. 3(b) and 3(d). The two very different

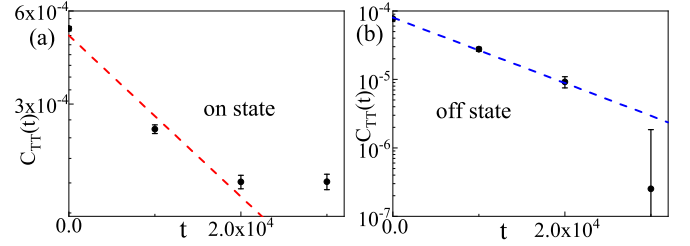


FIG. 4. Autocorrelation of the finite-time temperature in the (a) on and (b) off states. Dashed lines correspond to exponential decays, which are analytically expected.

ways of decay are induced by two entirely different underlying mechanisms, which are explained in Sec. IV.

D. Autocorrelation of the finite-time temperature $T_O(t)$

The correlation functions are quite valuable to determine the type of stochastic process and evaluate quantitatively the magnitude of fluctuations and return the strength of a stochastic system. Here we have calculated the autocorrelation of the finite temperature $T_O(t)$, i.e.,

$$C_{TT}(\tau) = \langle \Delta T_O(t) \Delta T_O(t + \tau) \rangle_t, \quad (14)$$

where $\Delta T_O(t) \equiv T_O(t) - \bar{T}_O(t)$, i.e., the value relative to its mean value. To clearly present the properties of the system, $C_{TT}(\tau)$ is calculated in the on and off states separately. Therefore, $\bar{T}_O(t)$, the mean value of $T_O(t)$, equals T_{on} and T_{off} for the on and off states, respectively.

Numerical results are depicted in Fig. 4. We see that the correlations decay very rapidly and thus their values drop to an undetectable level shortly. Two straight lines that correspond to exponential decays are also plotted for reference.

IV. THEORETICAL ANALYSES: OVERDAMPED BROWNIAN PARTICLE IN A DOUBLE-WELL POTENTIAL

To understand quantitatively the above observations, the properties of the noise terms in the Eq. (5) are crucial. Since little detail about these fluctuation terms is known and the correlation timescales of the fluctuation are much shorter than the timescales that we shall study, we simply suppose that they form Gaussian white noise, i.e., $\xi_J(t) \equiv \xi_L(t) + \xi_R(t) = \gamma \xi(t)$, where $\xi(t)$ denotes a standard Gaussian white noise which satisfies $\langle \xi(t) \rangle = 0$ and $\langle \xi(t_1) \xi(t_2) \rangle = \delta(t_1 - t_2)$, where γ is the noise strength. The dynamics of the system is then governed by the following Langevin equation:

$$C_O \frac{dT_O}{dt} = -\frac{dV(T_O)}{dT_O} + \gamma \xi(t). \quad (15)$$

$V(T_O)$ takes the double-well form illustrated in Fig. 1(c). The two wells and the peak in between are at T_{on} , T_{off} , and T_{SO} , respectively. In the absence of the noise term, they are the two stable fixed points and one unstable fixed point of the deterministic dynamics.

A. T_O dependence of the heat capacity C_O

Generally speaking, the parameters C_O and γ can depend on T_O , which makes the dynamics quite complicated. To cal-

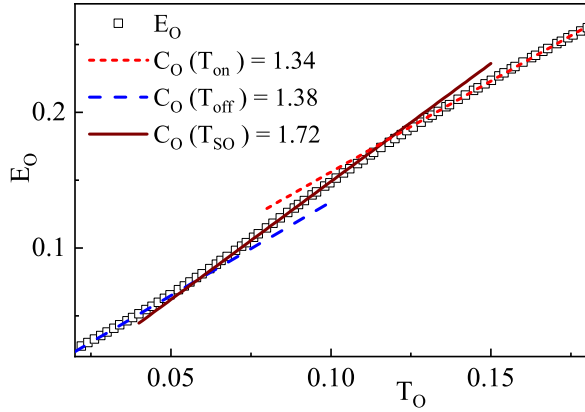


FIG. 5. Calorie curve of particle O . The running slope $\partial E_O/\partial T_O$ presents the heat capacity $C_O(T_O)$, which equals 1.34, 1.38, and 1.72 for $T_O = T_{\text{on}}$, T_{off} , and T_{SO} , respectively. Around each state, $C_O(T_O)$ is roughly independent of T_O .

culate the temperature dependence of C_O , we calculated the calorie curve of particle O and plotted it in Fig. 5. $\partial E_O/\partial T_O$, the running slope of the curves, has the value of C_O . We see that, around each steady state, C_O is basically a constant. $C_O = 1.34$, 1.38, and 1.72 around the on, off, and semi-on states, respectively. In the following analyses, we study the dynamics around the three key states separately, so C_O can be treated as a constant in each case.

As for the noise strength γ , theoretically speaking, it can be determined by the variances of the noise terms, which unfortunately cannot be calculated directly in the numerical simulations. Here we suppose similarly that it also is basically constant around each steady state. In future studies, this term will be studied in more detail.

B. Around the unstable steady state T_{SO}

1. PDF of finite-time temperature $T_O(t)$

Around the unstable steady state T_{SO} , the first-order approximation of Eq. (15) reads

$$\frac{dx^*}{dt} = \frac{\theta^*}{C_O} x^* + \frac{\gamma}{C_O} \xi(t), \quad (16)$$

whose dynamics of the probability density function $P(x^*, t)$ is governed by a Fokker-Planck equation (FPE):

$$\frac{dP}{dt} = -\frac{\theta^*}{C_O} \frac{\partial}{\partial x^*} (x^* P) + \frac{\gamma^2}{2C_O^2} \frac{\partial^2 P}{\partial x^{*2}}, \quad (17)$$

where $x^* \equiv T_O - T_{\text{SO}}$ and

$$\theta^* \equiv -\left. \frac{d^2 V(x^*)}{dx^{*2}} \right|_{x^*=0} = -\Delta J'(T_{\text{SO}}) > 0.$$

The stationary-state distribution of Eq. (17) follows

$$P(x^*) \sim e^{-\frac{C_O \theta^* x^{*2}}{\gamma^2}}, \quad (18)$$

which takes an inverted Gaussian form with variance $\sigma_{\text{SO}}^2 = \frac{\gamma^2}{2C_O \theta^*}$ in a single logarithmic plot. This explains well the

inverted Gaussian distribution observed in Fig. 2(b) and described in Eq. (9).

2. Lifetime distribution in short- τ regime

Furthermore, since around the unstable steady state, $dV(x^*)/dx^* \approx 0$, the above process roughly reduces to simple Brownian motion. Suppose at time $t = 0$, $x^* = 0$, the first-return time (FRT) τ , i.e., the first time that x^* returns to zero, can be regarded as the lifetime of a short-time stay in a SSS. Its probability density distribution, according to the Sparre-Andersen theorem [19], decays as

$$P_{\text{short}}(\tau) \sim \tau^{-\frac{3}{2}}. \quad (19)$$

This $-3/2$ power exponent agrees exactly with the power-law decay of the lifetime probability density in the short- τ regime observed in Figs. 3(a) and 3(c) and described in Eqs. (10) and (11).

C. Around a stable steady state T_{on} or T_{off}

1. PDF of finite-time temperature $T_O(t)$

On the other hand, around a stable steady state on or off, Eq. (15) reduces to a 1D Ornstein-Uhlenbeck (OU) process:

$$\frac{dx}{dt} = -\frac{\theta}{C_O} x + \frac{\gamma}{C_O} \xi(t), \quad (20)$$

where x denotes $T - T_{\text{on}}$ or $T - T_{\text{off}}$ and

$$\theta \equiv \left. \frac{d^2 V(x)}{dx^2} \right|_{x=0} = \Delta J'(T_{\text{on/off}}),$$

which takes positive values. The corresponding FPE reads

$$\frac{dP}{dt} = \frac{\theta}{C_O} \frac{\partial}{\partial x} (xP) + \frac{\gamma^2}{2C_O^2} \frac{\partial^2 P}{\partial x^2}. \quad (21)$$

The stationary solution follows:

$$P(x) = \sqrt{\frac{C_O \theta}{\pi \gamma^2}} e^{-\frac{C_O \theta x^2}{\gamma^2}}, \quad (22)$$

which takes a Gaussian form with variance

$$\sigma^2 = \frac{\gamma^2}{2C_O \theta}. \quad (23)$$

This explains well the Gaussian distributions observed in Figs. 3(a) and 3(c) and described in Eqs. (7) and (8).

2. Lifetime distribution in long- τ regime

Suppose a Brownian particle has already been far away from the unstable steady state, it would oscillate around one of the two SSSs for a long time, then the role of its prehistory vanishes, so the event that it returns again (by a rare chance) to the unstable fixed point with distance S follows a Poisson process. Consequently, the time interval between consecutive returns satisfies an exponential decay,

$$P_{\text{long}}(\tau) = \frac{1}{\tau_0} e^{-\tau/\tau_0}, \quad (24)$$

where τ_0 denotes the average duration time of these long-time stays. Such an exponential decay explains well the findings observed in Figs. 3(b) and 3(d) and described in Eqs. (12) and (13).

Consider a Brownian particle in a harmonic potential with height h and width $2S$. Suppose it is initially put at the bottom of the potential, then the mean first time that the particle reaches one end of the potential is expected to be

$$\tau_0 \sim \frac{(1 + \sqrt{\pi})C_O}{\theta} \int_0^{\frac{S\sqrt{C_O\theta}}{\gamma}} e^{t^2} dt. \quad (25)$$

A detailed derivation of Eq. (25) can be found in Ref. [20]. In this case, S corresponds to $T_{\text{on}} - T_c = 0.153 - 0.085 = 0.068$ and $T_c - T_{\text{off}} = 0.085 - 0.043 = 0.042$ for the on and off states, respectively. However, since this theoretical expectation depends too sensitively on the upper limit of the integral, it is very hard to obtain a good agreement with the numerically measured values of τ_0 .

3. Mean lifetime

Due to the existence of the short-time stays, the tail part of the overall lifetime distribution follows

$$P(\tau) = Ae^{-\tau/\tau_0}, \quad (26)$$

with the coefficient $A < 1/\tau_0$. The overall mean lifetime τ_{MEAN} is the average over both the short- and long-time stays, i.e.,

$$\tau_{\text{MEAN}} \equiv \frac{\sum_i \tau_i}{N}, \quad (27)$$

where τ_i denotes the lifetime of the i th stay and N denotes the total number of stays. Since the numerator is mainly contributed to by the long-time stays, we have

$$\tau_{\text{MEAN}} \approx \int_0^\infty A\tau e^{-\tau/\tau_0} d\tau = A\tau_0^2. \quad (28)$$

τ_{MEAN} for the on and off states calculated bases on the fittings in Figs. 3(b) and 3(d) are $4.0 \times 10^{-7} \times (1.15 \times 10^6)^2 = 5.29 \times 10^5$ and $5.0 \times 10^{-7} \times (1.01 \times 10^6)^2 = 5.10 \times 10^5$, respectively, which agree with the directly calculated values 5.32×10^5 and 5.10×10^5 very well. If this τ_{MEAN} is too short, then it is hard to study the properties of the two SSSs separately. Whereas, if τ_{MEAN} is too long, then the jumps from one SSS to the other SSS can hardly be observed by numerical simulations. The case in our previous study on thermal memory [6] belongs to the latter case. Although it works very well as a thermal memory, the mean lifetime (roughly 10^9) is too long for the present studies. That is why we designed another set of parameters in this paper.

4. Autocorrelation of temperature T_O

In such a stable steady state the autocorrelation of x is expected to be [21]

$$C_{xx}(t) \equiv \langle x(t_0)x(t_0 + t) \rangle_{t_0} = \frac{\gamma^2}{2C_O\theta} e^{-\frac{\theta}{C_O}|t|}, \quad (29)$$

which indicates an exponential decay. Here x corresponds to the relative finite-time temperature $\Delta T_O(t)$ shown in Eq. (14).

Its autocorrelations for the on and off states are plotted in Figs. 4(a) and 4(b), respectively. The decay is so rapid that it is quite hard to fit an exponent with satisfying accuracy, but the expected exponential type seems reasonable.

V. SUMMARY AND DISCUSSION

To summarize, the stochastic dynamics of a nonlinear thermal device with NDTR is studied. Due to the NDTR, there exist three steady states satisfying the continuity condition, two of which are stable and the other one in between is unstable. The system mostly walks around one SSS but thermal fluctuations can drive it occasionally from this SSS to the other SSS. In this work, such rare jumps have been directly observed by numerical simulations, and the probability density distribution of the finite-time temperature T_O of the key particle O , which well describes the state of the system, is also presented. It is observed that the PDF of T_O displays two peaks that locate at the two SSSs and a well that locates at the USS in between. Superior to existing studies [6,16], more details of the PDF, i.e., the scaling properties around each steady state, are quantitatively studied. We see around each SSS that the PDF displays a Gaussian distribution, while around the USS the distribution follows an inverted Gaussian form. Furthermore, the distribution $P(\tau)$ for the lifetime τ of each SSS is studied. $P(\tau)$ follows two completely different scaling laws in short- and long- τ regimes. A power-law decay $\tau^{-1.5}$ is observed in the short- τ regime, whereas in the long- τ regime the decay becomes exponential. Finally, the autocorrelation C_{TT} of T_O around each SSS has been calculated and exponential decays are observed.

By considering the thermal fluctuation of the heat currents, we propose a Langevin equation, which originally describes an overdamped Brownian particle that undergoes a double-well potential, and found that it describes suitably the stochastic dynamics of the system. The two wells correspond to the two above-mentioned SSSs and the local peak in between corresponds to the USS. All the aforementioned findings can then be explained. Around each well, the dynamics reduces to a 1D OU process and the corresponding linearized FPE expects a Gaussian asymptotic distribution, which explains the Gaussian-type PDF profile observed around each SSS. Meanwhile, around the local peak, the linearized FPE expects an inverted Gaussian distribution, which agrees again with the numerical observation around the USS. On the other hand, around the local peak of the potential the dynamics reduces to that of a simple Brownian particle, whose probability of the first return time $P(\tau)$ decays with τ as $\tau^{-1.5}$. While, for a particle initially placed in a SSS, the escape from the SSS follows a Poisson process and the probability of the first-passage time decays exponentially with τ . These facts are entirely consistent with the observed decays of $P(\tau)$ in the short- and long- τ regimes, respectively. Finally, the dynamics expects an exponentially decaying autocorrelations of the position of particle around each well, which explains the observed exponential decay of C_{TT} .

As a conclusion, all the observations of the thermal device with bistability agree very well with the theoretical expectations. The present study may deepen our understanding of the dynamics of a multiple-stable-steady-state system, thus

it is helpful in improving the performance of various thermal control devices such as thermal memory. The underlying mechanisms for NDTR may vary, but we believe that this study is also applicable to a number of other mechanisms that induce NDTR and bistability, not limited to the match and mismatch of phonon spectra. To describe the thermal systems more precisely, the detailed properties of thermal fluctuations might also be necessary. Further studies may be extended to it. Thermal multistability systems, which are even more complicated, may also be considered. Very recently, an approach of designing macroscopic bistability and multistability, which

applies to arbitrary diffusive systems, has been proposed [22]. The practical merits of the related studies can be naturally expected.

ACKNOWLEDGMENTS

This work was supported by the National Natural Science Foundation of China under Grant No. 12075316. Computational resources were provided by the Physical Laboratory of High Performance Computing at Renmin University of China.

-
- [1] S. Lepri, R. Livi, and A. Politi, Thermal conduction in classical low-dimensional lattices, *Phys. Rep.* **377**, 1 (2003); A. Dhar, Heat transport in low-dimensional systems, *Adv. Phys.* **57**, 457 (2008); A. Dhar, A. Kundu, and A. Kundu, Anomalous heat transport in one dimensional systems: A description using non-local fractional-type diffusion equation, *Front. Phys.* **7**, 159 (2019).
- [2] N. Li, J. Ren, L. Wang, G. Zhang, P. Hänggi, and B. Li, Colloquium: Phononics: Manipulating heat flow with electronic analogs and beyond, *Rev. Mod. Phys.* **84**, 1045 (2012).
- [3] M. Terraneo, M. Peyrard, and G. Casati, Controlling the Energy Flow in Nonlinear Lattices: A Model for a Thermal Rectifier, *Phys. Rev. Lett.* **88**, 094302 (2002); B. Li, L. Wang, and G. Casati, Thermal Diode: Rectification of Heat Flux, **93**, 184301 (2004); B. Li, J. H. Lan, and L. Wang, Interface Thermal Resistance between Dissimilar Anharmonic Lattices, *ibid.* **95**, 104302 (2005).
- [4] B. Li, L. Wang, and G. Casati, Negative differential resistance and thermal transistor, *Appl. Phys. Lett.* **88**, 143501 (2006).
- [5] L. Wang and B. Li, Thermal Logic Gates: Computation with Phonons, *Phys. Rev. Lett.* **99**, 177208 (2007).
- [6] L. Wang and B. Li, Thermal Memory: A Storage of Phononic Information, *Phys. Rev. Lett.* **101**, 267203 (2008).
- [7] D. He, S. Buyukdagli, and B. Hu, Origin of negative differential thermal resistance in a chain of two weakly coupled nonlinear lattices, *Phys. Rev. B* **80**, 104302 (2009); W.-R. Zhong, P. Yang, B.-Q. Ai, Z.-G. Shao, and B. Hu, Negative differential thermal resistance induced by ballistic transport, *Phys. Rev. E* **79**, 050103(R) (2009); Z.-G. Shao, L. Yang, H.-K. Chan, and B. Hu, Transition from the exhibition to the nonexhibition of negative differential thermal resistance in the two-segment frenkel-kontorova model, *ibid.* **79**, 061119 (2009); H.-K. Chan, D. He, and B. Hu, Scaling analysis of negative differential thermal resistance, *ibid.* **89**, 052126 (2014).
- [8] B. Hu, L. Yang, and Y. Zhang, Asymmetric Heat Conduction in Nonlinear Lattices, *Phys. Rev. Lett.* **97**, 124302 (2006); G. Casati, C. Mejia-Monasterio, and T. Prosen, Magnetically Induced Thermal Rectification, *ibid.* **98**, 104302 (2007); J. Ren and J.-X. Zhu, Asymmetric Andreev reflection induced electrical and thermal Hall-like effects in metal/anisotropic superconductor junctions, *Phys. Rev. B* **89**, 064512 (2014); G. Tang, X. Chen, J. Ren, and J. Wang, Rectifying full-counting statistics in a spin Seebeck engine, *ibid.* **97**, 081407(R) (2018); G. Tang, L. Zhang, and J. Wang, Thermal rectification in a double quantum dots system with a polaron effect, *ibid.* **97**, 224311 (2018); K. H. Lee, V. Balachandran, and D. Poletti, Giant rectification in segmented, strongly interacting spin chains despite the presence of perturbations, *Phys. Rev. E* **103**, 052143 (2021); K. H. Lee, V. Balachandran, C. Guo, and D. Poletti, Transport and spectral properties of the $xx + xxz$ diode and stability to dephasing, *ibid.* **105**, 024120 (2022); F. Li, H. Li, J. Wang, G. Xia, and G. Hwang, Tunable thermal rectification and negative differential thermal resistance in gas-filled nanostructure with mechanically-controllable nanopillars, *J. Therm. Sci.* **31**, 1084 (2022).
- [9] T. S. Komatsu and N. Ito, Thermal transistor utilizing gas-liquid transition, *Phys. Rev. E* **83**, 012104 (2011); A. Fornieri, G. Timossi, R. Bosisio, P. Solinas, and F. Giazotto, Negative differential thermal conductance and heat amplification in superconducting hybrid devices, *Phys. Rev. B* **93**, 134508 (2016); R. Sánchez, H. Thierschmann, and L. W. Molenkamp, All-thermal transistor based on stochastic switching, *ibid.* **95**, 241401(R) (2017); J. Ren, Predicted rectification and negative differential spin Seebeck effect at magnetic interfaces, *ibid.* **88**, 220406 (2013); Y. Zhang, Z. Yang, X. Zhang, B. Lin, G. Lin, and J. Chen, Coulomb-coupled quantum-dot thermal transistors, *Europhys. Lett.* **122**, 17002 (2018); P. Ben-Abdallah and S.-A. Biehs, Near-Field Thermal Transistor, *Phys. Rev. Lett.* **112**, 044301 (2014); F. Li, J. Wang, G. Xia, and Z. Li, Negative differential thermal resistance through nanoscale solid fluid solid sandwiched structures, *Nanoscale* **11**, 13051 (2019).
- [10] M. Buchanan, Fast bit-switching in a thermal memory, *Physics* **7**, 85 (2014); C. Guarcello, P. Solinas, A. Braggio, M. Di Ventura, and F. Giazotto, Josephson Thermal Memory, *Phys. Rev. Appl.* **9**, 014021 (2018); V. Kubytskyi, S.-A. Biehs, and P. Ben-Abdallah, Radiative Bistability and Thermal Memory, *Phys. Rev. Lett.* **113**, 074301 (2014).
- [11] C. W. Chang, D. Okawa, A. Majumdar, and A. Zettl, Solid-state thermal rectifier, *Science* **314**, 1121 (2006); C. W. Chang, D. Okawa, H. Garcia, A. Majumdar, and A. Zettl, Nanotube Phonon Waveguide, *Phys. Rev. Lett.* **99**, 045901 (2007); O.-P. Saira, M. Meschke, F. Giazotto, A. M. Savin, M. Mötönen, and J. P. Pekola, Heat Transistor: Demonstration of Gate-Controlled Electronic Refrigeration, *ibid.* **99**, 027203 (2007); W. Kobayashi, Y. Teraoka, and I. Terasaki, An oxide thermal rectifier, *Appl. Phys. Lett.* **95**, 171905 (2009); R. Xie, C. T. Bui, B. Varghese, Q. Zhang, C. H. Sow, B. Li, and J. T. L. Thong, An electrically tuned solid state thermal memory based on metal insulator transition of single crystalline VO₂

- nanobeams, *Adv. Funct. Mater.* **21**, 1602 (2011); K. Ito, K. Nishikawa, and H. Iizuka, Multilevel radiative thermal memory realized by the hysteretic metal-insulator transition of vanadium dioxide, *Appl. Phys. Lett.* **108**, 053507 (2016); A. M. Morsy, R. Biswas, and M. L. Povinelli, High temperature, experimental thermal memory based on optical resonances in photonic crystal slabs, *APL Photonics* **4**, 010804 (2019); T. Meng, Y. Sun, C. Tong, P. Zhang, D. Xu, J. Yang, P. Gu, J. Yang, and Y. Zhao, Solid-state thermal memory of temperature-responsive polymer induced by hydrogen bonds, *Nano Lett.* **21**, 3843 (2021); S. Pal and I. K. Puri, Thermal and gate using a monolayer graphene nanoribbon, *Small* **11**, 2910 (2015); S. N. Ahmed Hamed, Nanothermomechanical and and or logic gates, *Sci. Rep.* **10**, 2437 (2020); R. C. Ng, A. Castro Alvarez, and C. M. Sotomayor Torres, Thermal rectification and thermal logic gates in graded alloy semiconductors, *Energies (Basel, Switz.)* **15**, 4685 (2022).
- [12] B. Liang, W.-w. Kan, X.-y. Zou, L.-l. Yin, and J.-c. Cheng, Acoustic transistor: Amplification and switch of sound by sound, *Appl. Phys. Lett.* **105**, 083510 (2014).
- [13] J. S. Blakemore, A. E. de Barr, and J. B. Gunn, Semiconductor circuit elements, *Rep. Prog. Phys.* **16**, 160 (1953).
- [14] D. He, B.-q. Ai, H.-K. Chan, and B. Hu, Heat conduction in the nonlinear response regime: Scaling, boundary jumps, and negative differential thermal resistance, *Phys. Rev. E* **81**, 041131 (2010); W.-R. Zhong, M.-P. Zhang, B.-Q. Ai, and B. Hu, Anomalous negative differential thermal resistance in a momentum-conserving lattice, *ibid.* **84**, 031130 (2011); Y. Yang, D. Ma, Y. Zhao, and L. Zhang, Negative differential thermal resistance effect in a macroscopic homojunction, *J. Appl. Phys.* **127**, 195301 (2020). Y. Yang, X. Li, and L. Zhang, Bidirectional and unidirectional negative differential thermal resistance effect in a modified Lorentz gas model, *Chin. Phys. Lett.* **38**, 016601 (2021).
- [15] O. M. Braun and Y. S. Kivshar, Nonlinear dynamics of the Frenkel Kontorova model, *Phys. Rep.* **306**, 1 (1998).
- [16] Q. Ruan and L. Wang, Switchability and controllability of a thermal transistor, *Phys. Rev. Res.* **2**, 023087 (2020).
- [17] T. Mai, A. Dhar, and O. Narayan, Equilibration and Universal Heat Conduction in Fermi-Pasta-Ulam Chains, *Phys. Rev. Lett.* **98**, 184301 (2007).
- [18] L. Wang, S. Liu, and B. Li, Validity of local thermal equilibrium in anomalous heat diffusion, *New J. Phys.* **21**, 083019 (2019).
- [19] J. Klafter and I. M. Sokolov, *First Steps in Random Walks: From Tools to Applications* (Oxford University Press, Oxford, 2011).
- [20] A. J. F. Siegert, On the first passage time probability problem, *Phys. Rev.* **81**, 617 (1951); A. G. Nobile, L. M. Ricciardi, and L. Sacerdote, Exponential trends of Ornstein-Uhlenbeck first-passage-time densities, *J. Appl. Probab.* **22**, 360 (1985); L. M. Ricciardi and S. Sato, First-passage-time density and moments of the Ornstein-Uhlenbeck process, *ibid.* **25**, 43 (1988).
- [21] R. Kubo, Electronic properties of metallic fine particles. I., *J. Phys. Soc. Jpn.* **17**, 975 (1962); A. Rahman, Correlations in the motion of atoms in liquid argon, *Phys. Rev.* **136**, A405 (1964); R. Kubo, The fluctuation-dissipation theorem, *Rep. Prog. Phys.* **29**, 255 (1966); B. U. Felderhof, On the derivation of the fluctuation-dissipation theorem, *J. Phys. A: Math. Gen.* **11**, 921 (1978).
- [22] J. Wang, G. Dai, F. Yang, and J. Huang, Designing bistability or multistability in macroscopic diffusive systems, *Phys. Rev. E* **101**, 022119 (2020).